Electronic Supporting Information

Multimodal Control of Liquid Crystalline Mesophases from Surfactants with Photoswitchable Tails

Judith E. Houston,[ab]‡ Elaine A. Kelly,[b] Margarita Kruteva,[c] Kiriaki Chrissopoulou,[d] Nathan Cowieson[e] and Rachel C. Evans[f]*

[a] *Jülich Centre for Neutron Science (JCNS-4), Forschungszentrum Jülich GmbH, Lichtenbergstr. 1, 85748 Garching, Germany.*

[b] *School of Chemistry and CRANN, University of Dublin, Trinity College, College Green, Dublin 2, Ireland.*

[c] *Jülich Centre for Neutron Science (JCNS-1) and the Institute of Complex Systems (ICS-1), Forschungszentrum Jülich GmbH, Leo-Brandt-Str., 52425 Jülich, Germany.*

[d] *Institute of Electronic Structure and Laser, Foundation for Research and Technology – Hellas, P.O. Box 1527, 711 10, Heraklion, Crete, Greece.*

[e] *Diamond Light Source, Harwell Science and Innovation Campus, Didcot, Oxfordshire, OX11 0DE, United Kingdom.*

[f] *Department of Materials Science & Metallurgy, University of Cambridge, 27 Charles Babbage Road, Cambridge, CB3 0FS, United Kingdom.*

‡ Current address: European Spallation Source ERIC, Box 176, SE-221 00 Lund, Sweden.

* *Corresponding Author Email: rce26@cam.ac.uk*

Table of Contents

1 Instrumentation

1.1 Electrospray Ionisation Mass Spectrometry (ESI-MS)

ESI-MS were recorded by Dr Martin Feeney on a Bruker microTOF-Q III spectrometer interfaced to a Dionex UltiMate 3000 liquid chromatography system, in negative and positive modes as required. The instrument was calibrated using a tune mix solution (Agilent Technologies ESI-l low concentration tuning mix). Masses were recorded over the range 100-1200 *m*/*z*. Samples were prepared in HPLC grade solvent.

1.2 Fourier-Transform Infrared (FTIR) Spectroscopy

FTIR spectra were recorded on a Perkin-Elmer Spectrum 100 FTIR spectrometer using a universal attenuated total reflection (ATR) sampling accessory. All spectra were recorded at room temperature over the range 4000-650 cm^{-1}, with a resolution of 4 cm^{-1}. The following abbreviations are used to describe the intensities: s, strong; m, medium; w, weak and br, broad.

1.3 ^{1}H and ^{13}C Nuclear Magnetic Resonance (NMR) Spectroscopy

Solution NMR spectroscopy was performed by Dr John O'Brien on a Bruker DPX 400 NMR instrument at 20 °C. ^{1}H and ^{13}C NMR spectra were obtained using an operating frequency of 400 and 151 MHz, respectively. Chemical shifts were calibrated against a tetramethylsilane (TMS) signal and are reported in parts per million (ppm). $CDCl_3$ (δ_H = 7.26 ppm, singlet; δ_C = 77.16 ppm, triplet), D_2O (δ_H = 4.79 ppm, singlet) and d_6-DMSO (δ_H = 2.50 ppm, singlet; δ_C = 39.52 ppm, septuplet) were used as deuterated solvents.[1]

1.4 Melting Point Analysis

Measurements were performed on a Stuart SMP3 melting point apparatus. The heating block possesses 3 capillary tube holders. The heating rate was set at 0.5 °C min^{-1}.

1.5 Dynamic Light Scattering (DLS)

DLS measurements were performed using a Zetasizer Nano series nano-ZS instrument (Malvern Instruments, U.K.). The apparatus is equipped with a He-Ne laser (λ_{ex} = 633 nm, 4.0 mW power source). Detection of the scattering intensity was done at a backscattering angle of 173°. Millipore water was filtered 5 times, prior to preparation of the solutions. For each sample, three measurements were performed, each taking an average of 15 scans. Cumulant analysis of the autocorrelation function was used to determinate the polydispersity and the mean hydrodynamic diameter (*Z*-average) of each sample.

1.6 Surface Tensiometry (ST)

Surface tensiometry measurements were performed on a Kibron EZ-Pi^{plus} surface tensiometer using a DyneCups plastic cuvette (3 mL) and a DyneProbe ring. The instrument uses the Du Noüy–Padday method to record ST data. The method allows the interfacial force between two media to be determined. The obtained data were recorded on AquaPiPlus software and were averaged from 5 runs for each sample. Millipore water was used as a reference sample.

2 Synthesis and Characterisation

2.1 Materials

4-ethylaniline (98%), 4-butylaniline (97%), 4-octylaniline (99%), sodium nitrite ($NaNO_3$, ≥99.0%), 1,2-dibromoethane (98%), anhydrous potassium carbonate (≥99.0%), potassium iodide (KI, 99.0%), sodium sulfite (98%), copper sulfate pentahydrate (≥98.0%), ammonium hydroxide (5.01 M solution in water), hydroxylamine hydrochloride (98%), sodium hydride (60% w/w in mineral oil), potassium hydroxide (KOH, ≥85%), 1,6-dibromohexane (96%), 4-aminophenol (≥98.0%), diethylene glycol (99%), tetraethylene glycol (99%), hexaethylene glycol (97%) and hydrochloric acid (HCl, conc. 37%), ethanol (HPLC grade), tetrahydrofuran (THF, HPLC grade), diethyl ether (≥99.5%), dichloromethane, acetone and hexane were purchased from Sigma Aldrich. 4-hexylaniline (90%) was purchased from ChemCruz. Sodium hydroxide (NaOH, ≥97%) and chloroform (>99%) were purchased from Fisher Scientific and phenol (>99.0%) was purchased from BDH Chemical Ltd. England. 1,4-dibromobutane (>98%) and 1,8-dibromooctane (>98%) were purchased from Alfa Aesar. Trimethylamine (24% weight in water) was purchased from ACROS. All reagents and solvents were used as received unless otherwise stated.

2.2 General synthesis

The family of ethylene glycol azobenzene photosurfactants was synthesised in three steps: 1) the preparation of the hydroxyl azobenzene precursor, **1** (**C$_m$AzoOH**), with the desired alkyl tail length; 2) modification of **1** to a bromoprecursor, **2** (**C$_m$AzoOC$_n$Br**), incorporating the desired alkyl spacer; and 3) addition of the polar oligo(ethylene glycol) head group to form the final AzoPS (**C$_m$AzoOC$_n$E$_o$**), **3**. All intermediates and the final products were characterised by ^{1}H NMR, ^{13}C NMR, ESI-MS, melting point analysis and FTIR spectroscopy and compared to literature data.

2.2.1 *Synthesis of C_mAzoOH (4-alkyl-4-hydroxyl azobenzene, replace alkyl with ethyl (C_2AzoOH), butyl (C_4AzoOH), hexyl (C_6AzoOH) or octyl (C_8AzoOH) as appropriate for desired tail length)*

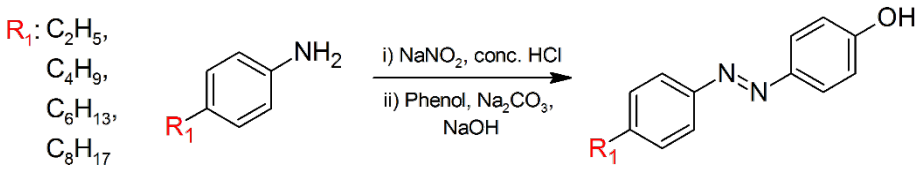

Scheme S1. Synthetic route to the hydroxyl-azobenzene precursor **C*m*AzoOH**, where *m* = 2, 4, 6 or 8.

In a round-bottomed flask (250 mL), 4-alkylaniline (20 mmol: 4-butylaniline, 1.5 g; 4-ethylaniline: 2.49 mL; 4-butylanine: 3.16 mL; 4-hexylaniline: 3.85 mL; 4-octylaniline: 4.57 mL) was dissolved in a 1:1 (*v*/*v*) acetone/H_2O mixture (50 mL) with HCl (37% conc., 4 mL) and stirred for 20 min in an ice bath. Separately, $NaNO_2$ (1.7 g, 20 mmol) was dissolved in distilled H_2O (25 mL) and cooled to 1-3 ºC. To the cooled (~ 2 ºC) 4-alkylaniline solution, the $NaNO_2$ solution was added slowly, and left for 20 min to stir in an ice bath to produce the diazonium salt. Additionally, phenol (1.9 g, 20 mmol), NaOH (0.8 g, 20 mmol) and Na_2CO_3 (2.1 g, 20 mmol) were dissolved in distilled H_2O (50 mL), stirred for 5 min and cooled to 1-3 ºC. To this solution, the resultant diazonium salt was added dropwise and the temperature was maintained below 8 ºC. For the ethyl, hexyl and octyl analogues, an aqueous NaOH solution (6.5 mL, 2.5 mmol L^{-1}) was added dropwise to the basic phenol solution along with the acidic diazonium salt solution, in order to maintain a final pH of 10. The resulting yellow/brown precipitates were left to cool to room temperature, filtered and washed with minimum amounts of cold acetone and cold distilled water. The product was recrystallised from chloroform to give yellow crystals with an average yield of 70%.

C_2AzoOH (1a)

^{1}H NMR ($CDCl_3$, 400 MHz, 25 °C): δ = 1.31 (t, J = 8 Hz, 3H), 2.75 (quart., J = 8 Hz, 2H), 6.96 (d, J = 8.8 Hz, 2H), 7.34 (d, J = 8.2 Hz, 2H), 7.82 (d, J = 8.3 Hz, 2H), 7.88 (d, J = 8.8 Hz, 2H) ppm.

^{13}C NMR ($CDCl_3$, 100 MHz, 25 °C): δ = 15.4, 28.8, 115.8, 122.6, 124.9, 128.5, 147.2, 150.9, 158.0 ppm.

FTIR: ν = 3163 (br.), 2960 (w), 2927 (m), 2848 (w), 1583 (s), 1505 (s), 1242 (s), 1131 (s) cm^{-1}.

Mass Spectrometry (CH_3Cl, m/z: APCI$^+$): Exact mass calculated: 226.1106 [M], Exacted mass obtained: 227.1168 $[M+H]^+$.

Melting Point: 85.1 – 86.2 °C.

Yield: 68%

C_4AzoOH (1b)

^{1}H NMR ($CDCl_3$, 400 MHz, 25 °C): δ = 0.93 (t, J = 8.0 Hz, 3H, CH_3); 1.30-1.43 (m, 2H, CH_2); 1.57-1.68 (m, 2H, CH_2); 2.71 (t, J = 8.0 Hz, 2H, CH_2); 5.17 (s, 1H, OH), 6.96 (d, J = 10.9 Hz, 2H, 2×CH); 7.32 (t, J = 10.9 Hz, 2H, 2×CH); 7.81 (d, J = 8.1 Hz, 2H, 2×CH); 7.88 (d, J = 8.1 Hz, 2H, 2×CH) ppm.

^{13}C NMR ($CDCl_3$, 100 MHz, 25 °C): δ = 13.98 (alkyl), 22.37 (alkyl), 33.51 (alkyl), 35.58 (alkyl), 114.69 (sp^2 Azo), 122.55 (sp^2 Azo), 124.67 (sp^2 Azo), 129.09 (sp^2 Azo), 145.89 (quart. Azo), 147.00 (quart. Azo), 150.94 (quart. Azo), 161.29 (quart. Azo) ppm.

ESI-MS (MeOH, *m/z*-ESI-): Calculated: 255.1453 $[M+H]^-$. Found: 255.1485 $[M+H]^-$.

FTIR ν_{max}: 3553 (s), 3180 (b), 2922 (b), 1748 (m), 1591 (m) cm^{-1}.

Melting Point: 102-115 ºC

Yield: 94%

C_6AzoOH (1c)

^{1}H NMR: ($CDCl_3$, 400 MHz, 25 °C): δ = 0.91 (t, J = 8 Hz, 3H), 1.34 (m, 6H), 1.68 (m, 2H), 2.67 (t, J = 9 Hz, 2H,), 5.06 (s, br.), 6.98 (d, J = 7 Hz, 2H), 7.33 (d, J = 8.4 Hz, 2H), 7.81 (d, J = 7.2 Hz, 2H), 7.88 (d, J = 8.4 Hz, 2H) ppm.

^{13}C NMR: ($CDCl_3$, 100 MHz, 25 °C): δ = 14.1, 22.6, 28.9, 31.3, 31.7, 35.9, 115.8, 122.5, 124.8, 129.1, 146, 147.2, 150.9, 158.2 ppm.

FTIR: ν = 3547 (w), 3292 (b), 2956 (s), 2916 (s), 2849 (s), 1646 (w), 1586 (s), 1478 (C-H, s), 1404 (, s), 1290 (s), 1142 (s), 830 (s) cm^{-1}.

Mass Spectrometry (CH_3Cl, m/z: APCI$^+$): Exact mass calculated: 282.1732 [M], exact mass obtained: 281.1659 $[M-H]^+$.

Melting Point: 86.9 – 88.8 °C.

Yield: 74%

C_8AzoOH (1d)

^{1}H NMR: ($CDCl_3$, 400 MHz, 25 °C): δ = 0.90 (t, J = 7 Hz, 3H), 1.33 (m, 8H), 1.66 (m, 4H), 2.69 (t, J = 7 Hz, 2H,), 5.5 (s, br.,), 6.96 (d, J = 7.2 Hz, 2H), 7.32 (d, J = 9 Hz, 2H), 7.81 (d, J = 7.2 Hz, 2H), 7.88 (d, J = 8.4 Hz, 2H) ppm.

^{13}C NMR: ($CDCL_3$, 100 MHz, 25 °C): δ = 14.2, 22.7, 29.3, 29.5, 31.3, 31.9, 35.9, 115.9, 122.5 125.1, 129.1, 146.1, 147.1, 150.6, 158.3 ppm.

FTIR: ν = 3427 (br), 2956 (s), 2923 (s), 2856 (s), 1586 (s), 1465 (s), 1243 (s), 1135 (s), 833 (s), 558 (s) cm^{-1}.

Mass Spectrometry (CH_3Cl, m/z: APCI$^+$): Exact mass calculated: 310.2045 [M], exact mass obtained: 309.1977 $[M-H]^+$.

Melting Point: 87.2 – 88.8 °C.

Yield: 66%

2.2.2 *Synthesis of bromoprecursor CmAzoOCnBr (4-alkyl-4'(4/6/8-bromo)alkoxy azobenzene, replace alkyl with ethyl, butyl, hexyl and octyl as relevant, and select 4/6/8 accordingly)*

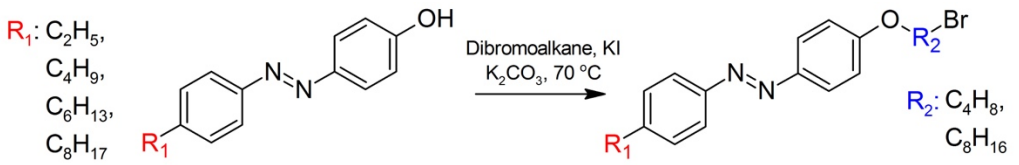

Scheme S2. Synthetic route to the bromide precursor **C$_m$AzoOC$_n$Br**, where m = 2, 4, 6 or 8 and n = 4 or 8.

In a round-bottomed flask (50 mL), C_4AzoOH (4.0 g, 14 mmol) was dissolved in acetone (160 mL). To this solution, 2 equivalents of 1,4-dibromobutane (18 g, 9.8 mL, 69 mmol), anhydrous potassium carbonate (excess – 6.7 g, 47 mmol) and a catalytic amount of potassium iodide (2.0 g, 13.5 mmol) were added. The reaction mixture was refluxed at 65 ºC and stirred for 20 h. The yellow/red solution was allowed to cool to RT, the excess salt was removed *via* filtration and the solvent removed under reduced pressure. The solid was dissolved in hexane (~30 mL) and washed with water until the washings became clear. The hexane was removed by rotary evaporation. The excess of 1,4-dibromobutane was removed using a silica plug and washed several times with cyclohexane. The product was collected with dichloromethane (DCM) and dried under vacuum. The products were recrystallised from ethanol to give yellow crystals with an average yield of ~80%.

For the synthesis of C_2AzoOC_4Br, C_2AzoOH (1 eq., 10 mmol, 2.26 g) was dissolved in acetone (25 mL). 1,4 di-bromobutane (2 eq., 20mmol, 2.39 mL), K_2CO_3 (2 eq., 20 mmol, 2.76 g) and KI (0.1 eq., 1 mmol, 0.17 g) were added to the reaction flask and the resulting dark red solution was stirred under reflux at 65 °C for 2 days with monitoring *via* thin layer chromatography (TLC, 9:1 cyclohexane: ethyl acetate). When the reaction reached completion, acetone was removed *via* rotary evaporation and the product was dissolved in dichloromethane (DCM, 20 mL) and washed with water several times to remove the co-salt. DCM was removed *via* rotary evaporation and C_2AzoOC_4Br was recovered as an orange solid upon recrystallization from ethanol.

For the synthesis of C_6AzoOC_4Br and C_8AzoOC_4Br the appropriate hydroxyl precursor (1 eq., 10 mmol, C_6AzOH: 2.82 g, C_8AzoOH: 3 g) was reacted with 1,4-dibromobutane (2 eq., 20 mmol, 2.39 mL) as outlined above for C_2AzoOC_4Br. For the synthesis of C_8AzoOC_8Br, C_8AzoOH (1 eq., 10 mmol, 3.1 g) was reacted with 1,8 di-bromooctane (2 eq., 20 mmol, 3.68 mL) as outlined above for C_2AzoOC_4Br.

C_2AzoOC_4Br (2a)

^{1}H NMR: ($CDCl_3$, 400 MHz, 25 °C): δ = 1.31 (t, J = 8 Hz, 3H), 2.02 (m, 2H), 2.13 (m, 2H), 2.74 (m, J = 8 Hz, 2H), 3.53 (mt, J = 6 Hz, 2H), 4.11 (t, J = 6, Hz 2H), 7.01 (d, J = 9 Hz, 2H) 7.34 (d, J = 8.36 Hz, 2H) 7.83 (d, J = 8.32 Hz, 2H) 7.92 (d, J = 9 Hz, 2H) ppm.

^{13}C NMR: ($CDCl_3$, 400 MHz, 25 °C): δ = 15.4, 27.8, 28.82, 29.4, 33.4, 67.2, 114.7, 122.6, 124.6, 128.5, 147.1, 147.1, 151, 161.1 ppm.

FTIR: ν = 2966 (w), 2920 (m), 2861 (w), 1609 (s), 1497 (s), 1236 (s), 1138 (s) cm^{-1}.

Mass Spectrometry: (CH_3Cl, m/z: $APCI^+$): Exact mass calculated: 360.0837 [M], exact mass obtained: [M+H] 361.0910.

Melting Point: 115.4 – 117.3 °C

Yield: 82%

C_4AzoOC_4Br (2b)

^1H NMR (DMSO, 400 MHz, 25 °C): δ = 0.92 (t, J = 7.3 Hz, 3H, CH_3); 1.33-1.42 (m, 2H, CH_2); 1.60-1.67 (m, 2H, CH_2); 1.84-1.94 (m, 2H, CH_2) ; 1.96-2.05 (m, 2H, CH_2); 2.67 (t, J = 7.8 Hz, 2H, CH_2); 3.64 (t, 2H, J = 6.6 Hz, CH_2); 4.13 (t, 2H, J = 6.2 Hz, CH_2); 7.13 (d, 2H, J = 8.9 Hz, 2×CH); 7.39 (d, 2H, J = 8.3 Hz, 2×CH); 7.77 (d, 2H, J = 8.3 Hz, 2×CH); 7.87 (d, 2H, J = 9.0 Hz, 2×CH) ppm.

^{13}C NMR (DMSO, 100 MHz, 25 °C): δ = 14.24 (alkyl), 19.03 (alkyl), 22.22 (alkyl), 27.78 (alkyl). 33.39 (alkyl), 35.11 (alkyl), 56.49 (alkyl), 67.59 (alkyl), 115.50 (sp^2 Azo), 122.74 (sp^2 Azo), 124.86 (sp^2 Azo), 129.68 (sp^2 Azo), 146.17 (quart. Azo), 146.62 (quart. Azo), 150.74 (quart. Azo), 161.59 (quart. Azo) ppm.

ESI-MS ($CHCl_3$, *m/z*-ESI+): Found: 389.1225 $[M+H]^+$. Calculated: 389.1223 $[M+H]^+$.

FTIR ν_{max}: 3462 (w), 2965 (br), 1765 (m), 1375 (m), 1208 (m) cm^{-1}.

Melting Point: 62-64 ºC.

Yield: 96% (5.2 g, 13.4 mmol)

C_6AzoOC_4Br (2c)

^1H NMR: ($CDCl_3$, 400 MHz, 25 °C): δ = 0.92 (t, J = 8 Hz, 3H), 1.35 (m, 6H), 1.68 (m, 2H), 2.06 (m, 4H), 2.7 (t, J = 6.6 Hz, 2H), 3.47 (m, 2H), 4.11 (t, J = 6 Hz, 2H) 7.03 (d, J = 8.8 Hz, 2H), 7.29 (d, J = 8.2 Hz), 7.81 (d, J = 8.3 Hz 2H), 7.9 (d, J = 8.9 Hz, 2H) ppm.

^{13}C NMR: **($CDCl_3$, 400 MHz, 25 °C):** δ = 14.1, 22.62, 27.9, 29, 31, 31.3, 32.5, 33.4, 35.9, 67.2, 119.7, 122.6, 124.6, 129.1, 145.9, 147.1, 151, 161.1 ppm.

FTIR: ν = 2914 (s), 2848 (w), 1602 (s), 1498 (s), 1380 (w), 1256 (s), 1133 (s) cm^{-1}.

Mass Spectrometry (CH_3Cl, m/z: APCI): Exact mass calculated: 416.1463 [M], exact mass obtained: 417.154 $[M+H]^+$

Melting Point: 136.2 - 137.5 °C

Yield: 85%

C_8AzoOC_4Br (2d)

^1H NMR: ($CDCl_3$, 400 MHz, 25 °C): δ = 0.91 (t, J = 7 Hz, 3H) 1.3 (m, 10H), 1.66 (m, 2H), 2.02 (m, 2H), 2.11 (m, 2H), 2.7 (t, J = 8 Hz, 2H), 3.54 (t, J = 7 Hz, 2H) 4.11 (t, J = 7 Hz, 2H), 7.01 (d, J = 8.9 Hz, 2H), 7.32 (d, J= 8.2 Hz, 2H), 7.82 (d, J = 8.2 Hz, 2H), 7.92 (d, J = 8.9 Hz, 2H) ppm.

^{13}C NMR: ($CDCl_3$, 100 MHz, 25 °C): δ = 14.1, 22.7, 27.9, 29.2, 29.3, 29.4, 29.5, 31.3, 31.9, 33.4, 35.9, 67.2, 114.7, 122.5, 124.6, 129.1, 145.9, 147.1, 151.2, 161.1 ppm.

FTIR: ν = 2929 (s), 2838 (m), 1606 (s), 1498 (m), 1452 (m), 1393 (w), 1250 (s), 1141 (s) cm^{-1}.

Mass Spectrometry (CH_3Cl, m/z: APCI): Exact mass calculated: 444.1776 [M], exact mass obtained: 445.1849 $[M+H]^+$.

Melting Point: 138.4 – 140.1 °C

Yield: 67%

C_8AzoOC_8Br (2e)

^{1}H NMR: ($CDCl_3$, 400 MHz, 25 °C): δ = 0.91 (t, J = 8 Hz, 3H), 1.29-1.35 (m, 10H), 1.4 – 1.47 (m, 8H), 1.66 (quint., 2H), 1.86 (m, 4H), 2.69 (t, J = 7 Hz, 2H), 3.44 (m, 2H), 4.05 (t, J = 7 Hz, 2H), 7.01 (d, J= 9 Hz, 2H), 7.32 (d, J = 8.5 Hz, 2H), 7.81 (d, J = 8.6 Hz, 2H), 7.9 (d, J = 8.7 Hz, 2H) ppm.

^{13}C NMR: ($CDCl_3$, 100 MHz, 25 °C): δ = 14.1, 26, 29.2, 28.1, 28.5, 28.6, 28.7, 29.3, 29.3, 29.5, 31.4, 31.9, 32.7, 33.9, 35.9, 68.3, 114.7, 122.5, 124.6, 129.1, 145.8, 147, 151.1, 161.4 ppm.

Mass Spectrometry (CH_3Cl, m/z: APCI$^+$): Exact mass calculated: 500.2402 [M], exact mass obtained: 501.2473 $[M+H]^+$.

Melting Point: 119.8 - 121.2 °C

Yield: 80%

2.2.3 2.2.3 Synthesis of $C_mAzoOC_nE_o$ (alkyl-(di-/tetra-/hexa-ethylene glycol) alkoxy azobenzene)

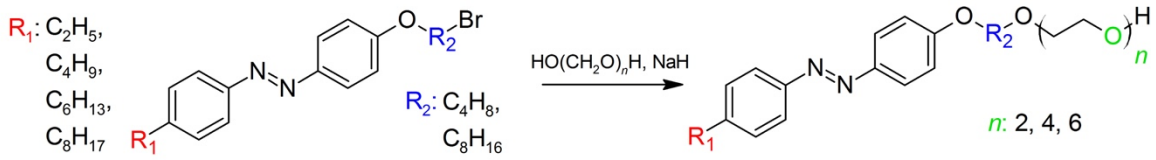

Scheme S3. Synthetic route to the neutral photosurfactants, **$C_4AzoOC_4E_2$**, **$C_2AzoOC_4E_4$**, **$C_4AzoOC_4E_4$**, **$C_6AzoOC_4E_4$**, **$C_8AzoOC_4E_4$**, **$C_8AzoOC_8E_4$** and **$C_4AzoOC_4E_6$**.

The corresponding ethylene glycol (~5 mL) was dried azeotropically by distillation with toluene (20 mL) at 170 ºC. Sodium hydride (NaH, 60% in mineral oil) (1 molar equivalents (eq.)) was reacted with dry ethylene glycol (4 eq.) in dry tetrahydrofuran (THF) at room temperature for 2 h under N_2 protection. Upon addition of the NaH, the solutions immediately bubbled and became foamy. **C_mAzoOC_nBr** (0.1 eq.) was dissolved in dry THF and added dropwise to the reaction mixture, which turned yellow. The mixture was refluxed at 75 ºC under N_2 for at least 48 h and monitored *via* thin layer chromatography (TLC) using ethyl acetate as the mobile phase. Ethylene glycol and product spots were developed on the TLC plate using potassium permanganate. Upon reaction completion, the solvent was removed by rotary evaporation. The dark red oil obtained was dissolved in dichloromethane and washed with water. The DCM layer was then dried with $MgSO_4$, filtered and the solvent removed by rotary evaporation. In some cases, unreacted **C_mAzoOC_nBr** was removed using a silica plug and washed several times with chloroform. The final products were washed thoroughly with methanol and the solvent was removed by rotary evaporation. The structures of the all photosurfactants were confirmed by ^{1}H NMR, ^{13}C NMR, ESI-MS and IR spectroscopy. The data for the known surfactant, **$C_4AzoOC_4E_2$**, was compared to the literature data.[2] Spectroscopic and analytical data are summarised below.

$C_2AzoOC_4E_4$ (3a)

^{1}H NMR: ($CDCl_3$, 400 MHz, 25 °C): δ = 1 (t, J = 8 Hz, 3H), 1.81 (m, 2H), 1.9 (m, 2H), 1.98 (m, 2H), 2.74 (t, J = 8 Hz, 2H), 3.65 (m, 16H) 4.09 (t, J = 6 Hz, 2H), 7.01 (d, J = 8.92 Hz, 2H), 7.33 (d, J = 8.24 Hz, 2H), 7.82 (d, J = 8.24 Hz, 2H), 7.9 (d, J = 8.92 Hz, 2H) ppm.

^{13}C NMR: ($CDCL_3$, 600 MHz, 25 °C): δ = 15.5, 26, 26.1, 28.8, 61.7, 68, 70.2-70.9 (7 peaks) 72.64, 114.69, 122.6, 124.6, 128.49, 146.97, 147.04, 151.05, 161.38 ppm.

FTIR: v = 3404 (br.), 2965 (w), 2933 (s), 2874 (w), 1589 (s), 1492 (m), 1249 (s), 1315 (s) cm^{-1}.

Mass Spectrometry (CH_3Cl, m/z: APCI$^+$): Exact mass calculated: 474.2730. Exact mass obtained: 475.2779 $[M+H]^+$.

Yield: 38%

$C_4AzoOC_4E_2$ (3b)[2]

^{1}H NMR ($CDCl_3$, 400 MHz, 25 °C): δ = 0.93 (t, 3H, J = 7.4 Hz, CH_3), 1.32-1.42 (m, 2H, J = 7.4 Hz CH_2), 1.59-1.67 (m, 2H, CH_2), 1.75-1.85 (m, 4H, 2×CH_2), 1.86-1.95 (m, 2H, J = 6.8 Hz, CH_2), 2.67 (t, 2H, J = 7.9 Hz, CH_2), 3.56 (t, 2H, J = 6.3 Hz, CH_2), 3.59-3.76 (m, 9H, 4×CH_2), 4.07 (t, 3H, J = 6.3 Hz, CH_3), 6.99 (d, 2H, J = 9.0 Hz, 2×CH), 7.29 (d, 2H, J = 8.3 Hz, 2×CH), 7.83 (d, 2H, J = 8.3 Hz, 2×CH), 7.93 (d, 2H, J = 9.3 Hz, 2×CH) ppm.

^{13}C NMR ($CDCl_3$, 100 MHz, 25 °C): δ = 14.07 (alkyl), 22.46 (alkyl), 33.57 (alkyl), 35.69 (alkyl), 61.96 (alkyl linker), 68.14 (alkyl linker), 71.09 (alkyl linker), 72.63 (alkyl linker), 70.41 (glycol chain), 70.63 (glycol chain), 114.90 (sp^2 Azo), 122.69 (sp^2 Azo), 125.19 (sp^2 Azo), 129.24 (sp^2 Azo), 146.04 (quart. Azo), 146.66 (quart. Azo), 156.46 (quart. Azo), 161.62 (quart. Azo) ppm.

ESI-MS (MeOH, *m/z*-ESI+): Found: 437.2416 $[M+Na]^+$. Calculated: 437.2416 $[M+Na]^+$; Found: 415.2599 $[M+H]^+$. Calculated: 415.2597 $[M+H]^+$; Found: 452.2165 $[M+K]^+$. Calculated: 452.2156 $[M+K]^+$.

FTIR ν_{max}: 3462 (br), 2941 (s), 2867 (s), 1734 (s), 1599 (m), 1513 (m), 1376 (m), 1263 (s), 1094 (m), 835 (m) cm^{-1}.

Yield: 35% (370 mg, 0.89 mmol)

$C_4AzoOC_4E_4$ (3c)

^{1}H NMR ($CDCl_3$, 400 MHz, 25 °C): δ = 0.94 (t, 3H, J = 7.4 Hz, CH_3), 1.32-1.43 (m, 2H, J = 7.7 Hz, CH_2), 1.59-1.68 (m, 2H, CH_2), 1.75-1.84 (m, 4H, 2×CH_2), 1.86-1.95 (m, 2H, J = 6.8 Hz, CH_2), 2.68 (t, 2H, J = 7.9 Hz, CH_2), 3.56 (t, 2H, J = 6.7 Hz, CH_2), 3.58-3.75 (m, 16H, 2×4CH_2), 4.08 (t, 3H, J = 6.3 Hz, CH_3), 7.00 (d, 2H, J = 9.0 Hz, 2×Ar CH), 7.30 (d, 2H, J = 8.3 Hz, 2×CH), 7.83 (d, 2H, J = 8.3 Hz, 2×CH), 7.94 (d, 2H, J = 9.3 Hz, 2×CH).

^{13}C NMR ($CDCl_3$, 100 MHz, 25 °C): δ = 13.97 (alkyl), 22.36 (alkyl), 26.01 (alkyl), 26.11 (alkyl), 33.48 (alkyl), 35.59 (alkyl), 61.72 (alkyl linker), 68.08 (alkyl linker), 70.14 (glycol chain), 70.22 (glycol chain), 70.53-70.61 (glycol chain), 70.95 (glycol chain), 72.66 (glycol chain), 114.81 (sp^2 Azo), 122.58 (sp^2 Azo), 125.03 (sp^2 Azo), 129.13 (sp^2 Azo), 146.07 (quart. Azo), 146.51 (quart. Azo), 150.42 (quart. Azo), 161.78 (quart. Azo) ppm.

ESI-MS (MeOH, *m/z*-ESI+): Found: 501.2959 $(M^+ -H)^+$. Calculated: 501.2965 $(M^+ -H)^+$; Found: 503.3128 $(M^+ +H)^+$. Calculated: 503.3121 $(M^+ +H)^+$; Found: 525.2930 $(M^+ +Na)^+$. Calculated: 525.2941 $(M^+ +Na)^+$.

FTIR ν_{max}: 3457 (br), 2931 (s), 2861 (s), 1740 (s), 1603 (m), 1510 (m), 1364 (m), 1263 (m), 1115 (br), 831 (m) cm^{-1}.

Yield: 23.0% (300 mg, 0.6 mmol)

$C_4AzoOC_4E_6$ (3d)

^{1}H NMR ($CDCl_3$, 400 MHz, 25 °C): δ = 0.97 (t, 3H, J = 7.5 Hz, CH_3), 1.34-1.46 (m, 2H, CH_2), 1.62-1.72 (m, 2H, CH_2), 1.78-2.87 (m, 4H, 2×CH_2), 2.71 (t, 2H, J = 7.5 Hz, CH_2), 3.55-3.80 (m, 19H, 9×CH_2 and OH), 4.10 (t, 3H, J = 6.0 Hz, CH_2), 7.02 (d, 2H, J = 9.0 Hz, 2×CH), 7.33 (d, 2H, J = 9.0 Hz, 2×Ar CH), 7.84 (d, 2H, J = 6.0 Hz, 2×CH), 7.94 (d, 2H, J = 9.0 Hz, 2×CH).

^{13}C NMR ($CDCl_3$, 100 MHz, 25 °C): δ = 13.98 (alkyl), 22.35 (alkyl), 33.49 (alkyl), 35.56 (alkyl), 61.76 (alkyl linker), 68.06 (alkyl linker), 70.16 (alkyl linker), 72.68 (alkyl linker), 70.60 (glycol chain), 114.67 (sp^2 Azo), 122.51 (sp^2 Azo), 124.57 (sp^2 Azo), 129.06 (sp^2 Azo), 145.78 (quart. Azo), 147.00 (quart. Azo), 151.02 (quart. Azo), 161.36 (quart. Azo) ppm.

ESI-MS (MeOH, *m/z*-ESI+): Found: 589.3486 $[M-H]^+$. Calculated: 589.3489 $[M-H]^+$; Found: 591.3656 $[M+H]^+$. Calculated: 591.3645 $[M+H]^+$; Found: 613.3466 $[M+Na]^+$. Calculated: 613.3465 $[M+Na]^+$.

Yield: 37.0% (350 mg, 0.59 mmol)

$C_6AzoOC_4E_4$ (3e)

^{1}H NMR: ($CDCl_3$, 400 MHz, 25 °C): δ = 0.9 (t, J = 8 Hz, 3H), 1.22 (d, 2H), 1.33 (m, 6H), 1.66-1.9 (m, 6H), 2.69 (t, J = 8 Hz, 2H), 3.63 (m, 16H), 4.09 (t, J = 7 Hz, 2H), 7 (d, J = 8.88 Hz, 2H), 7.3 (d, J = 8.16 Hz, 2H), 7.8 (d, J = 8.2 Hz, 2H), 7.89 (d, J = 8.8 Hz, 2H) ppm.

^{13}C NMR: ($CDCl_3$, 600 MHz, 25 °C): δ = 14.1, 22.6, 26.1, 28.9, 30.9, 31.3, 31.7, 35.4, 61.7, 68, 70-70.9 (7 peaks), 72.65, 114.68, 122.51, 124.55, 129.03, 145.8, 146.9, 151, 161.4 ppm

FTIR: ν = 3175 (br.), 2959 (w), 2926 (m), 2873 (w), 1603 (s), 1490 (m), 1256 (s), 1131 (m) cm^{-1}.

Mass Spectrometry (CH_3Cl, m/z: APCI$^+$): Exact mass calculated: 530.3356. Exact mass obtained: 531.3442 $[M+H]^+$.

Yield: 39%

$C_8AzoOC_4E_4$ (3f)

^{1}H NMR: ($CDCl_3$, 400 MHz, 25 °C): δ = 0.79 (t, J = 8 Hz, 3H), 1.18-1.23 (m, 12H), 1.55 (m, 2H), 1.71 (m, 2H), 1.8 (m, 2H), 2.57 (t, J = 8 Hz, 2H), 3.49 (m, 12H), 3.62 (m, 4H), 3.97 (t, J = 8 Hz, 2H), 6.9 (d, J = 8.92 Hz, 2H), 7.2 (d, J = 8.24 Hz, 2H), 7.7 (d, J = 8.2 Hz, 2H), 7.78 (d, J = 8.88 Hz, 2H) ppm.

^{13}C NMR: ($CDCl_3$, 600 MHz, 25 °C): δ = 14, 22.6, 26, 25.9, 29.2, 29.4, 30.7, 31.2, 31.8, 35.73, 61.4, 67.9, 70-70.8 (7 peaks), 72.5, 114.3, 122.7, 124.5, 129.0, 145.2, 146.8, 151.1, 160.9 ppm.

FTIR: ν = 3175 (br.), 2965 (w), 2926 (m), 2866 (w), 1596 (s), 1497 (s), 1248 (s), 1135 (s) cm^{-1}.

Mass Spectrometry (CH_3Cl, m/z: APCI$^+$): Exact mass calculated: 558.3669. Exact mass obtained: 559.3714 $[M+H]^+$.

Yield: 42%

$C_8AzoOC_8E_4$ (3g)

H^1 NMR: ($CDCl_3$, 400 MHz, 25°C): δ = 0.84 (t, J = 8 Hz, 3H), 1.26 – 1.54 (m, 24H), 1.78 (m, 2H), 2.63 (t, J = 8 Hz, 2H), 3.64 (m, 16 H), 3.99 (t, J = 7 Hz, 2H), 6.95 (d, J = 9 Hz, 2H), 7.25 (d, J = 8.32 Hz, 2H), 7.75 (d, J = 8.36 Hz, 2H), 7.84 (d, J = 8.96 Hz, 2H) ppm.

C^{13} NMR: ($CDCl_3$, 600 MHz, 25°C): δ = 14.06, 22.61, 25.93, 29.2, 29.3, 29.2, 29.3, 29.3, 29.3, 30.9, 31.3, 31.8, 33.6, 35.8, 61.5, 68.3, 70.2-70 (7 peaks), 72.8, 114.6, 122.5, 124.5, 129, 145.8, 146.9, 151, 161.1 ppm.
FTIR: ν = 3169 (br.), 2971 (w), 2928 (m), 2867 (w), 1594 (s), 1498 (s), 1247 (s), 1139 (s) cm^{-1}.
Mass Spectrometry (CH_3Cl, m/z: $APCI^+$): Exact mass calculated: 614.4295 [M]. Exact mass obtained: 615.439 $[M+H]^+$.
Yield: 47%

3 Critical Micelle Concentrations

The critical micelle concentrations (*cmc*s) of AzoPS in water (20 °C) were determined for the *trans*- and *cis*-isomers using surface tensiometry (ST) and dynamic light scattering (DLS). In ST the *cmc* is reached when the surface tension becomes independent of surfactant concentration. While for DLS the intensity of scattering light increases significantly upon the onset of micelle formation.

Table S1. Critical micelle concentrations (*cmc*s) of the *trans*- and *cis*-isomers of the AzoPS determined using dynamic light scattering (DLS) and surface tensiometry (ST). The associated errors are given in brackets (standard deviation of three measurements).

AzoPS	***cmc* by ST** ($\times 10^{-6}$ mol L^{-1})		***cmc* by DLS** ($\times 10^{-6}$ mol L^{-1})	
	trans-isomer	*cis*-isomer	*trans*-isomer	*cis*-isomer
$C_2AzoOC_4E_4$	52.2 (2.4)	56.8 (2.1)	34.4 (5.7)	34.1 (19.1)
$C_4AzoOC_4E_4$	2.0	2.4	3.1	3.4
$C_6AzoOC_4E_4$	37.1 (6.3)	29.5 (1.8)	22.9 (4.2)	23.7 (5)
$C_8AzoOC_4E_4$	17.8 (2.1)	19.9 (1.8)	11.4 (1.6)	12.4 (1.2)
$C_4AzoOC_4E_6$	2.0	3.0	4.9	5.4
$C_4AzoOC_4E_2$	12.4	47.0	2.4	4.7
$C_8AzoOC_8E_4$	108.6 (3.1)	125.9 (2.3)	102.7 (33.9)	12.4 (1.2)

4 Packing Parameter Calculations

The nature of lyotropic liquid crystalline phase formed can be predicted from the viewpoint of the packing parameter,[3] $P = V/a_e l_c$, where V is volume of the hydrophobic tail, a_e is the area occupied by headgroups at the hydrophilic/hydrophobic interface, and l_c is the length of the hydrocarbon tail. The value of the packing parameter determines the predicted structure formed: <1/3, spherical micelles (*e.g.* cubic structure); 1/3 – 1/2, cylindrical micelles (two-dimensional hexagonal); 1/2 - 1, flexible bilayers (vesicles); and ≈1, planar bilayers (lamellar). In order to calculate the packing parameter of AzoPS, V and l_c were determined by the empirical volume additivity rule of Traube:[4]

$$V = \sum V_i \quad \textbf{Eq. S1}$$

$$l_c = \sum l_{ci} \quad \textbf{Eq. S2}$$

where V_i and l_{ci} are the contributions of the ith components. For AzoPS, the pendant alkyl chain, the azobenzene core, the oxy group and the spacer contributions are summed to obtain the total volume (Table S2). The method is repeated for the length (l_c).

The Tanford equations are commonly used to calculate the lengths and volumes of alkyl chain of surfactants[5] and were used to obtain the contributions of the alkyl chain of AzoPS.

$$V = 26.9 \times m + 27.4 \quad \textbf{Eq. S3}$$

$$l = 1.265 \times m + 1.5 \quad \textbf{Eq. S4}$$

where m is the number of -CH_2- carbons in the carbon chain. The contributions from the oxy group (V_3 and l_3) were obtained by *ab initio* calculations.[4, 6] The length of the azobenzene moiety is 0.9 nm and 0.55 nm for the *trans*- and *cis*-isomers, respectively.[7-11] The molecular volumes of the *trans*- and *cis*-isomers of the azobenzene core were obtained from computational calculation of the van der Waals volume and estimated to be 0.176 nm^3 and 0.177 nm^3, respectively.[12] Finally, although the effective surface areas, a_e, of oligooxyethylene polar headgroups are difficult to determine[13] and are known to be dependent on the hydrophobic chain,[13] these values can be approximated from the literature.[14, 15] Despite these assumptions, a reasonable estimation of the packing parameters (P) for AzoPS can be obtained and are summarized in Table S3.

Table S2. Contribution of volumes, lengths and effective areas to calculate the packing parameter, *P,* using the additivity principle.

Contributions	Values	Method
Alkyl chain volume (nm^3)	$0.0269m + 0.0274$	Tanford equations
Azobenzene volume (nm^3)	0.176/0.177 (*trans*/*cis*)	MOPAC calculations, van der Waals volume[12]
Oxy-group volume (nm^3)	9.1×10^{-3}	*Ab initio* calculations, van der Waals volume[4]
Alkyl chain length (nm)	$0.1265m + 0.15$	Tanford equation[5]
Azobenzene length (nm)	0.9/0.55 (*trans/cis*)	From X-Ray analysis[9]
Oxy-group length (nm)	0.28	DFT calculations[6]
E_2 effective area (nm^2)	0.35	ST study of $C_{12}E_2$ at 25 °C[14]
E_4 effective area (nm^2)	0.46	ST study of $C_{12}E_4$ at 25 °C[14]
E_6 effective area (nm^2)	0.52	ST study of $C_{12}E_6$ at 25 °C[15]

Table S3. Packing parameters (*P*) of the AzoPS in H_2O in the *trans*-isomeric forms.

AzoPS	Packing parameter
$C_2AzoOC_4E_4$	0.385
$C_4AzoOC_4E_4$	0.393
$C_6AzoOC_4E_4$	0.401
$C_8AzoOC_4E_4$	0.406
$C_4AzoOC_4E_6$	0.348
$C_4AzoOC_4E_2$	0.516
$C_8AzoOC_8E_4$	0.415

5 Small-Angle X-ray Scattering and Polarised Optical Microscopy

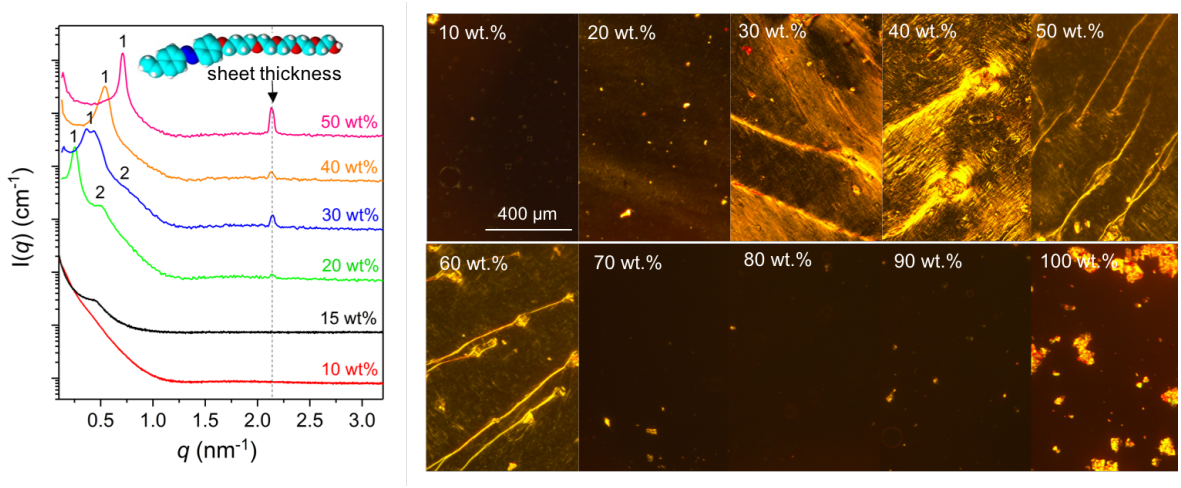

Figure S1. Small-angle X-ray scattering curves and polarised optical micrographs of *trans*-$C_2AzoOC_4E_4$ as a function of concentration at T = 20 °C.

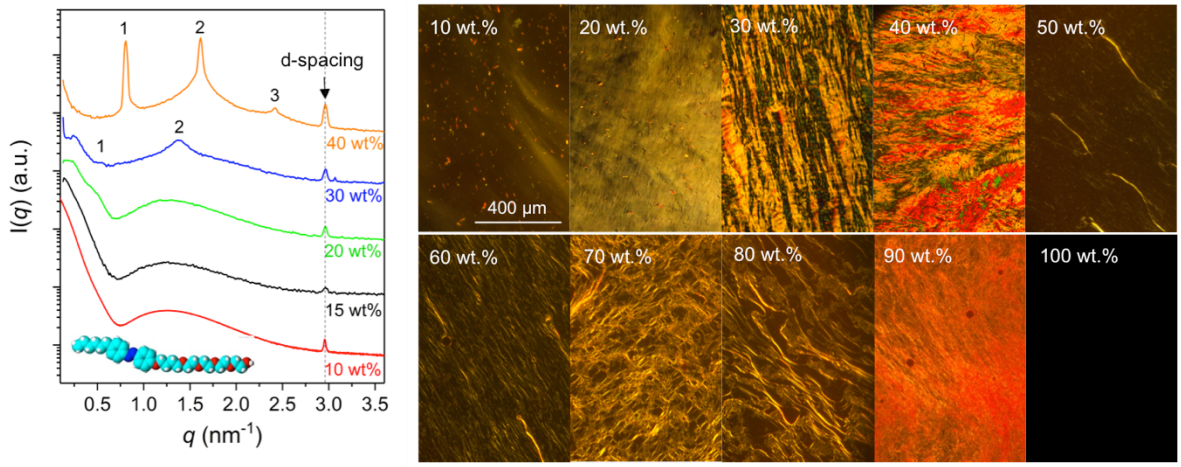

Figure S2. Small-angle X-ray scattering patterns and polarised optical micrographs of *trans*-$C_6AzoOC_4E_4$ as a function of concentration at T = 20 °C.

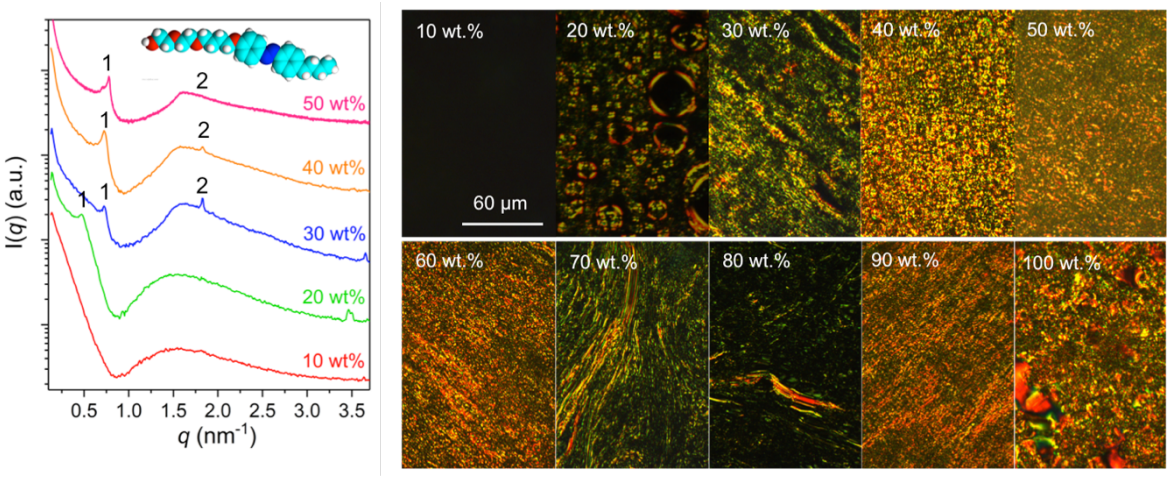

Figure S3. Small-angle X-ray scattering patterns and polarised optical micrographs of *trans*-$C_4AzoOC_4E_2$ as a function of concentration at T = 20 °C.

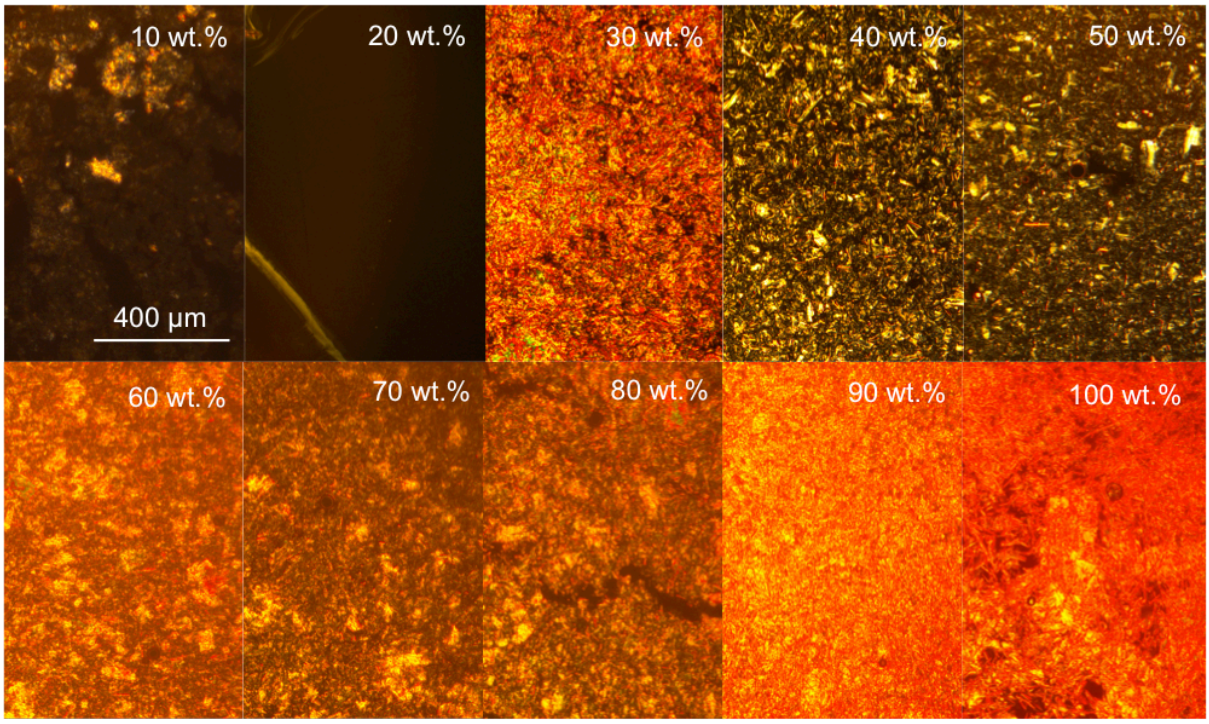

Figure S4. Polarised optical micrographs of *trans*-$C_8AzoOC_8E_4$ as a function of concentration at T = 20 °C. At all concentrations investigated, the images show a crystalline-like texture. Complete loss of birefringence was observed for all samples at 35 °C, presumably when the crystals had dissolved.

Table S4. Lattice parameters of the lamellar and hexagonal LLC phases AzoPS determined from SAXS.

AzoPS	Concentration (wt%)	Phase[ab]	Q_1 (nm^{-1})	Lattice constant (nm)
$C_2AzoOC_4E_4$	20	L_α	0.26	24.2
	30	L_α	0.37-0.44	14.3-17.0
	40	L_α	0.53	11.9
	50	L_α	0.71	8.8
$C_4AzoOC_4E_2$	30	H_I	0.73	9.9
	40	H_I	0.73	9.9
	50	H_I	0.73	9.9
$C_6AzoOC_4E_4$	20	H_I	0.21	34.5
	30	H_I	0.25	29.0
	40	H_I	0.80	9.1
$C_8AzoOC_4E_4$	50 [c]	H_I	0.82	8.8
	50 [c]	L_α	0.56	11.2
$C_4AzoOC_4E_6$	20	L_α	0.40	15.7
	30	L_α	0.49	12.8
	40	L_α	0.56	11.2
	50	L_α	0.89	7.1
$C_4AzoOC_4E_4$	10	L_α	0.34	18.5
	20	L_α	0.48	13.1
	30	L_α	0.81	7.8
	40	L_α	1.04	6.0
	50	L_α	0.97	6.5

[a] The interparticle distances for the lamellar sheets, $d_L = 2\pi/Q_1$, where Q_1 is the primary peak. [b] The interparticle distance in the hexagonal phase, $a_L = 4\pi/(\sqrt{3}*Q_1)$. [c] Two phases were observed in this sample: hexagonal phase and a second set of smaller peaks corresponding to the lamellar phase.

6 Hyperswollen Lamellar Phases

Table S5. Approximate alkyl chain (C_m)/ethylene glycol (E_n) ratios of each photosurfactant. Hyperswollen lamellar phases have previously been reported for neutral surfactants when a certain C_m/E_n ratio is reached (2.4 - 4).[16]

AzoPS	C_m/E_n	Value
$C_2AzoOC_4E_4$	12/4	3
$C_4AzoOC_4E_4$	14/4	3.5
$C_6AzoOC_4E_4$	16/4	4
$C_8AzoOC_4E_4$	18/4	4.5
$C_4AzoOC_4E_6$	14/6	2.3
$C_4AzoOC_4E_2$	14/2	7
$C_8AzoOC_8E_4$	22/4	5.5

7 Photoisomerisation Studies

UV/Vis absorption spectroscopy was employed to confirm that the azobenzene photosurfactants (AzoPS) undergo photoisomerisation. Similar optical properties were observed for all AzoPS, therefore, $C_4AzoOC_4E_6$ in H_2O at 20 °C is given as a representative example in Figure S5a. The photograph in Figure S5b highlights the significant change in colour from yellow to orange induced by the *trans*-to-*cis* isomerisation. The optical properties for all seven AzoPS are summarised in Table S5. When stored in the dark, AzoPS exist in the *trans*-form, which is thermodynamically more stable than the *cis*-form (>50 kJ mol^{-1}).[17] The *trans*-form of the AzoPS exhibits a maximum absorbance at λ_{abs} = ~340 nm (Figure S5a, blue line), which corresponds to the $\pi \rightarrow \pi^*$ transition.[18] Upon irradiation with UV-light (λ_{ex} = 365 nm) for 3 min, the *trans*-absorption band decreases significantly and two new bands appear, which are both assigned to the *cis*-form (red line, Figure S5a) at λ_{abs} = 314 nm ($\pi \rightarrow \pi^*$ transition) and λ_{abs} = 436 nm ($n \rightarrow \pi^*$ transition) for $C_4AzoOC_4E_6$.[19] No further changes in the absorption spectra were observed at longer illumination times (up to 40 min). However, it is important to note that the complete conversion to the *cis*-form cannot be obtained experimentally. An equilibrium known as the photostationary state (PSS) is obtained, which is comprised of a mixed population of *trans*- and *cis*-isomers.[20] Consequently, the *cis*-absorption spectrum contains a contribution from the *trans*-form. The *trans*-to-*cis* ratio in the PSS at λ_{abs} = 365 nm can be estimated by calculating the isomerisation degree (*ID*) from UV/Vis absorption spectroscopy using:[20]

$$ID = \frac{A_0(365) - A_i(365)}{A_0(365)} \times 100\% \qquad \textbf{Eq. S5}$$

where $A_0(365)$ is the absorbance at λ_{abs} = 365 nm before UV-light irradiation and $A_i(365)$ is the absorbance at the same wavelength measured at the PSS after irraditation.[21] Most of the AzoPS gave *ID*, summarized in Table S5, of between 84% and 95%, which correspond well to the literature values for similar non-ionic photosurfactants (86-89%).[20] The *ID*s for $C_4AzoOC_4E_2$ and $C_8AzoOC_8E_4$ are slightly lower than expected at ~68% and ~61%, respectively.

The reverse *cis*-to-*trans* isomerisation process was investigated by irradiation with blue light (λ_{ex} = 465 nm) for 3 min (Figure S5a, black line). For all AzoPS, incomplete recovery of the *trans*-form was observed. The absorbance of each AzoPS at λ_{abs} = 365 nm was found to only recover to 87-97% of their original values. This suggests the formation of a second photostationary state, where the *trans*-form is now the major isomer. Storage in the dark for 2 weeks was found to recover the original "dark" spectra.

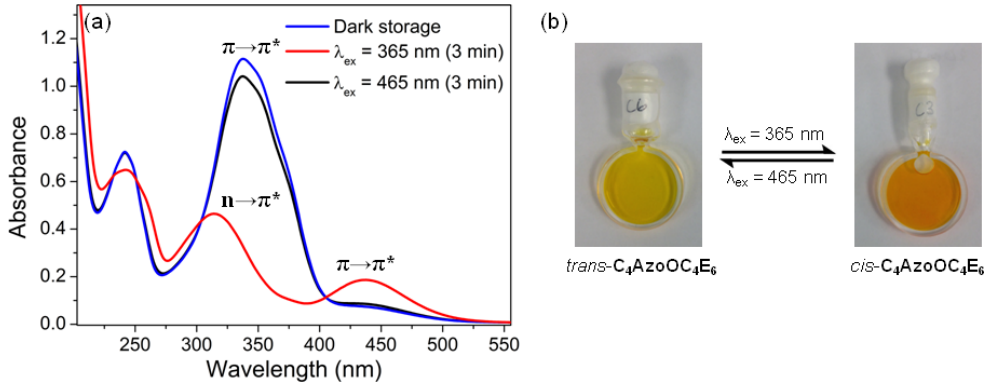

Figure S5. (a) UV/Vis absorption spectra of $C_4AzoOC_4E_6$ in water (3.4×10^{-5} M) at 20 °C. The spectra correspond to the *trans*-form (stored in the dark, blue line), the photostationary state (after irradiation at λ_{ex} = 365 nm for 3 min, red line) and the reverse *cis*- to *trans*-isomerisation (after irradiation at λ_{ex} = 465 nm for 3 min, black line). (b) Photographs of a concentrated solution of $C_4AzoOC_4E_6$ in water (2.0×10^{-2} M) before and after irradiation with UV light.

Table S6. UV/Vis absorption properties of the photosurfactants $C_2AzoOC_4E_4$ (6.5×10^{-5} M), $C_4AzoOC_4E_4$ (8.0×10^{-5} M), $C_6AzoOC_4E_4$ (6.5×10^{-5} M), $C_8AzoOC_4E_4$ (6.5×10^{-5} M), $C_4AzoOC_4E_6$ (3.4×10^{-5} M), $C_4AzoOC_4E_2$ (9.7×10^{-5} M) and $C_8AzoOC_8E_4$ (6.5×10^{-5} M), at 25 °C. ε_{trans} is the molar absorption coefficient for the *trans*-isomer and λ_{max} is the wavelength at which an absorption maximum is seen. $ID_{trans\text{-}cis}$ and $ID_{cis\text{-}trans}$ are the isomerisation degrees for the *trans*-*cis* and *cis*-*trans* processes.

AzoPS	ε_{trans} [a] (L mol^{-1} cm^{-1})	*trans*-λ_{max} (nm)	*cis*-λ_{max} (nm)	$ID_{trans\text{-}cis}$ (%)	$ID_{cis\text{-}trans}$ (%)
$C_2AzoOC_4E_4$	12,350	348	312, 438	89.6	87.7
$C_4AzoOC_4E_4$	15,800	334	317, 438	85.1	87.4
$C_6AzoOC_4E_4$	15,640	331	308, 443	84.1	95.2
$C_8AzoOC_4E_4$	15,874	332	308, 445	87.0	90.2
$C_4AzoOC_4E_6$	14,806	337	314, 436	84.5	92.0
$C_4AzoOC_4E_2$	10,714	324	313, 437	67.7	96.8
$C_8AzoOC_8E_4$	12,306	332	308, 443	61.1	93.7

[a] ε_{trans} was determined at 360 nm for $C_4AzoOC_4E_2$, $C_4AzoOC_4E_4$, and $C_4AzoOC_4E_6$ and at 332 nm for $C_2AzoOC_4E_4$, $C_6AzoOC_4E_4$, $C_8AzoOC_4E_4$, and $C_8AzoOC_8E_4$.

8 Kinetics Study of Photo- and Thermal-Isomerisation Processes

The rates of the forward and reverse photoisomerisation processes in dilute solution were also investigated for $C_4AzoOC_4E_2$, $C_4AzoOC_4E_4$ and $C_4AzoOC_4E_6$. The AsoPS in their *trans*-form were illuminated with UV-light (λ_{ex} = 365 nm) and the absorption spectra were simultaneously recorded every 30 s for a total duration of 6 min. The resulting spectra of the *trans*-*cis* photoconversion are shown in Figure S6a for $C_4AzoOC_4E_4$. A rapid *trans*-*cis* isomerisation is observed within the first 100 s. Further illumination increased the concentration of the *cis*-form until the photostationary state is reached (at ~3 min.), thereafter, conversion remained constant. To induce the reverse *cis*-to-*trans* process, the AzoPS in the *cis*-form were illuminated with blue-light (λ_{ex} = 465 nm) and the absorption spectra were simultaneously recorded every 5 s over a total duration of 1 min (Figure S6b for $C_4AzoOC_4E_4$).

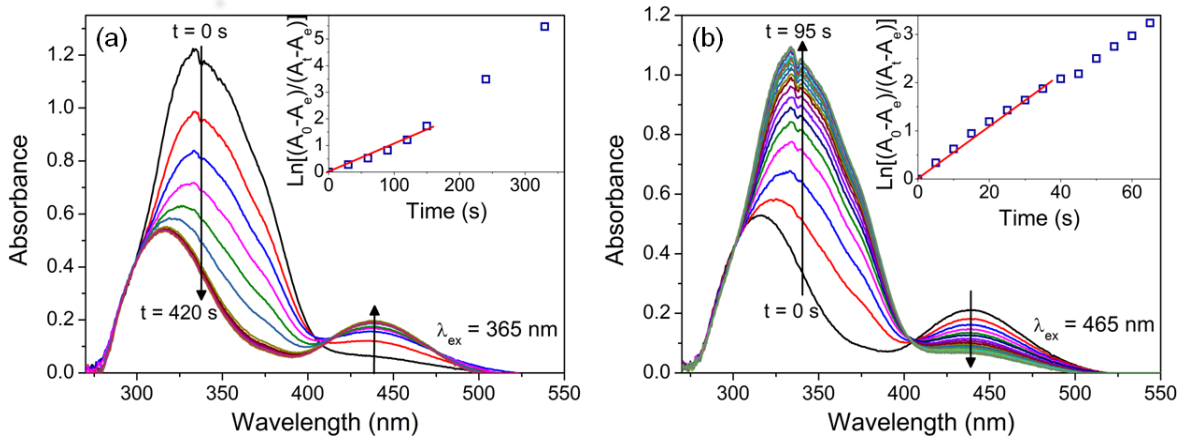

Figure S6. UV/Vis absorption spectra of $C_4AzoOC_4E_4$ in water (8.0×10^{-5} M), at 20 °C as a function of time under (a) UV-light irradiation (λ_{ex} = 365 nm) and (b) blue light irradiation (λ_{ex} = 465 nm). The insets show the first order rate laws for the forward (*trans-cis*) and reverse (*cis-trans*) isomerisation, respectively. The corresponding rate constants, k_{cis}, and k_{trans}, were obtained as described in the text.

The *trans*-to-*cis* (and *cis*-to-*trans*) photoisomerisation obey first-order kinetics, whose rate constant is given by:[22]

$$k_{cis}t = \left[\frac{A_0(365) - A_\infty(365)}{A_t(365) - A_\infty(365)}\right] \qquad \textbf{Eq. S6}$$

where k_{cis} is the rate constant describing the *trans-cis* isomerisation, $A_0(365)$ is the absorption at λ_{abs} = 365 nm of the *trans*-isomer before UV irradiation, $A_\infty(365)$ is the absorbance at the photostationary state and $A_t(365)$ is the absorbance at time, t. Equation S6 can be used to yield k_{cis} for the isomerisation of the AzoPS, as shown in the insets of Figure S6a for $C_4AzoOC_4E_4$. The reverse *cis*-to-*trans* isomerisation is described by the rate constant, k_{trans}, and can be determined experimentally by following the growth of the *trans*-isomer at λ_{abs} = 365 nm. The experimentally determined rate constants (k_{cis} and k_{trans}) obtained for the AzoPS are listed in Table S6.

Table S7. Photoisomerisation kinetics of the photosurfactants $C_4AzoOC_4E_2$ (9.7×10^{-5} M), $C_4AzoOC_4E_4$ (8.0×10^{-5} M) and $C_4AzoOC_4E_6$ (3.4×10^{-5} M) at 25 °C. k_{cis} and k_{trans} are the rate constants for *trans-cis* and *cis-trans* processes.

AzoPS	k_{cis} [a] (s^{-1})	k_{trans} [a] (s^{-1})
$C_4AzoOC_4E_4$	0.0111	0.0514
$C_4AzoOC_4E_6$	0.0152	0.0622
$C_4AzoOC_4E_2$	0.0035	0.0256

[a] The power outputs of the UV and blue LEDs were ~2.6 and 2.4 mW cm^{-2}, respectively, at a distance of 4.5 cm.

The lifetime of photoconversion (τ) can be deduced from the rate constant (*i.e.* $\tau_{cis} = 1/k_{cis}$ and $\tau_{trans} = 1/k_{trans}$). The calculated values are, τ_{cis} = 285, 90 and 66 s and τ_{trans} = 39, 19 and 17 s for $C_4AzoOC_4E_2$,

$C_4AzoOC_4E_4$ and $C_4AzoOC_4E_6$, respectively. There is an obvious correlation between the length of the hydrophilic ethylene glycol head-group and the lifetime of photoconversion as both processes proceed the fastest for the longer $C_4AzoOC_4E_6$. Electron-donating groups (EDG), such as the oxyethylene units, result in a modest decrease in the energy barrier for isomerisation.[18] Thus, it is not surprising that the AzoPS which the large EDG, $C_4AzoOC_4E_6$ has the shortest lifetimes.

The reverse *cis*-to-*trans* process can also proceed thermally, which is why the *trans*-form will be recovered from a solution of *cis*-isomers after a couple of days of storage in the dark. To quantify the thermal rate constant for *cis*-to-*trans* isomerisation, the UV/Vis absorption spectra of *cis*-$C_4AzoOC_4E_6$ was measured as a function of time while being heated to 20 and 60 °C (not shown). The calculated rate constants, k_{trans}^{T}, were 1.4×10^{-5} and 6.4×10^{-4} s^{-1} for 20 and 60 °C, respectively, both significantly lower than the rate of photoisomerisation (1.52×10^{-2} s^{-1}).

9 SAXS and *cis*-Isomers

Unfortunately, it was not possible to perform SAXS measurements of the AzoPS in their *cis*-forms for two reasons. Firstly, irradiating with the X-ray beam seemed to accelerate the reverse isomerisation to the *trans*-dominant form, as shown in the UV/Vis absorption spectra of two *cis*-samples measured directly before and after SAXS measurements on B21 (Diamond, UK), see Figure S7. Secondly, it was found that upon photoisomerisation with UV light, in some cases, AzoPS were phase separating, as seen the polarised optical micrograph in Figure 6b in the main article. Therefore, any conclusions about the structure of the *cis*-isomeric phases could only be drawn from the loss of birefringence in the POM measurements.

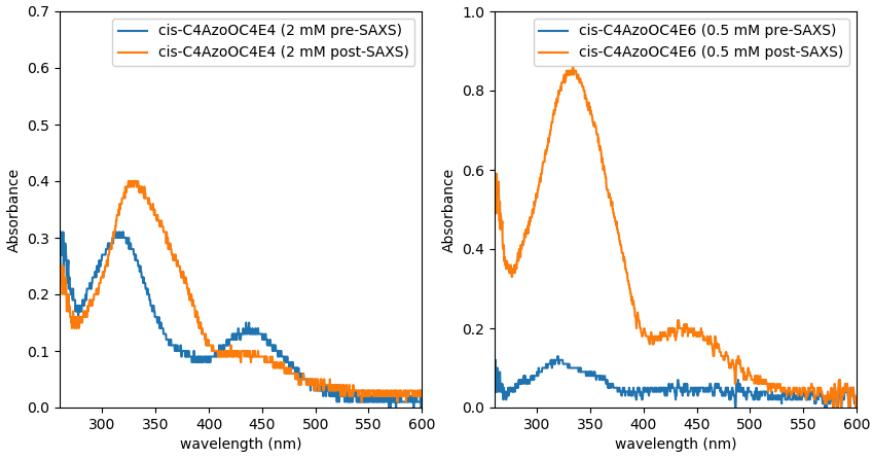

Figure S7. UV/Vis absorption spectra of (a) *cis*-$C_4AzoOC_4E_4$ (2 mM) and (b) *cis*-$C_4AzoOC_4E_6$ (0.5 mM) before (blue) and after (orange) the SAXS measurements on B21 (Diamond, UK).

10 Binary Temperature-Concentration Phase Diagrams

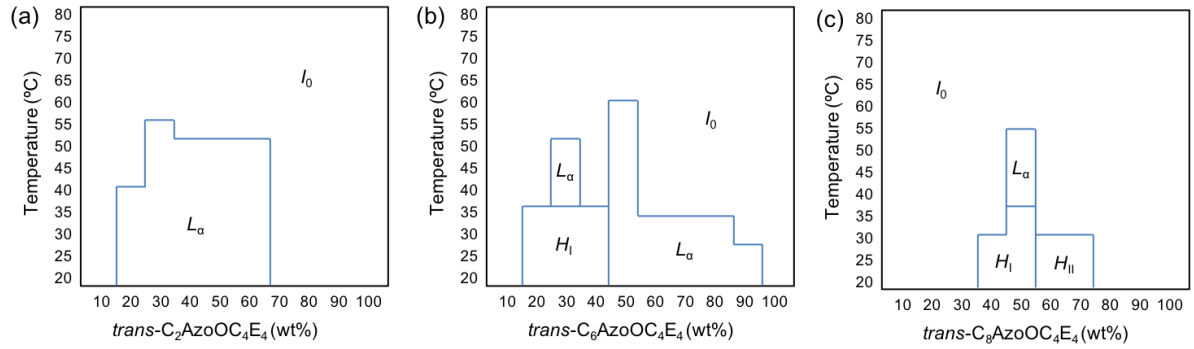

Figure S8. Temperature-concentration phase diagrams of the *trans*-isomers of a) C_2AzoOC$_4$E$_4$, b) C_6AzoOC$_4$E$_4$ and c) C_8AzoOC$_4$E$_4$ as a function of concentration and temperature. I_0, L_α, H_I and H_{II} represent the isotropic, lamellar and the normal and inverted hexagonal liquid crystalline phases, respectively.

11 References

1. H. E. Gottlieb, V. Kotlyar and A. Nudelman, *J. Org. Chem.*, 1997, **62**, 7512-7515.
2. T. Shang, K. A. Smith and T. A. Hatton, *Langmuir*, 2006, **22**, 1436-1442.
3. J. N. Israelachvili, D. J. Mitchell and B. W. Ninham, *J. Chem. Soc., Faraday Trans. 2*, 1976, **72**, 1525-1568.
4. H. Durchschlag and P. Zipper, in *Ultracentrifugation*, ed. M. D. Lechner, Steinkopff, Darmstadt, 1994, pp. 20-39.
5. C. Tanford, *J. Phys. Chem.*, 1972, **76**, 3020-3024.
6. F. Agapito, B. J. C. Cabral and J. A. M. Simões, *Journal of Molecular Structure: THEOCHEM*, 2005, **719**, 109-114.
7. R. F. Tabor, R. J. Oakley, J. Eastoe, C. F. J. Faul, I. Grillo and R. K. Heenan, *Soft Matter*, 2009, **5**, 78-80.
8. G. S. Kumar and D. C. Neckers, *Chem. Rev.*, 1989, **89**, 1915-1925.
9. E. Merino and M. Ribagorda, *Beilstein J. Org. Chem.*, 2012, **8**, 1071-1090.
10. G. C. Hampson and J. M. Robertson, *J. Chem. Soc. (Resumed)*, 1941, 409-413.
11. M. Sato, T. Kinoshita, A. Takizawa and Y. Tsujita, *Macromolecules*, 1988, **21**, 1612-1616.
12. K. Takeshita, N. Hirota and M. Terazima, *J. Photochem. Photobiol. A: Chem.*, 2000, **134**, 103-109.
13. R. Nagarajan, *Langmuir*, 2002, **18**, 31-38.
14. M. J. Rosen, A. W. Cohen, M. Dahanayake and X. Y. Hua, *J. Phys. Chem.*, 1982, **86**, 541-545.
15. M. Carvell, D. G. Hall, I. G. Lyle and G. J. T. Tiddy, *Faraday Discuss. Chem. Soc.*, 1986, **81**, 223-237.
16. Y. Uchida, T. Nishizawa, T. Omiya, Y. Hirota and N. Nishiyama, *J. Am. Chem. Soc.*, 2016, **138**, 1103-1105.
17. K. G. Yager and C. J. Barrett, *J. Photochem. Photobiol. A*, 2006, **182**, 250-261.
18. H. M. D. Bandara and S. C. Burdette, *Chem. Soc. Rev.*, 2012, **41**, 1809-1825.
19. Y. Zakrevskyy, J. Roxlau, G. Brezesinski, N. Lomadze and S. Santer, *J. Chem. Phys.*, 2014, **140**, 044906.
20. S. Peng, Q. Guo, P. G. Hartley and T. C. Hughes, *J. Mater. Chem. C*, 2014, **2**, 8303-8312.
21. S. Guo, K. Matsukawa, T. Miyata, T. Okubo, K. Kuroda and A. Shimojima, *J. Am. Chem. Soc.*, 2015, **137**, 15434-15440.
22. P. Sierocki, H. Maas, P. Dragut, G. Richardt, F. Vögtle, L. De Cola, F. Brouwer and J. I. Zink, *J. Phys. Chem. B*, 2006, **110**, 24390-24398.